OPEN ACCESS
IOP Publishing
Modelling and Simulation in Materials Science and Engineering
Modelling Simul. Mater. Sci. Eng. **30** (2022) 074003 (22pp) https://doi.org/10.1088/1361-651X/ac8c5e

Phase field crystal model for particles with *n*-fold rotational symmetry in two dimensions

Robert F B Weigel and Michael Schmiedeberg*

Institut für Theoretische Physik, Friedrich-Alexander-Universität Erlangen-Nürnberg, Staudtstr. 7, 91058 Erlangen, Germany

E-mail: michael.schmiedeberg@fau.de

Received 31 March 2022, revised 5 August 2022
Accepted for publication 24 August 2022
Published 8 September 2022

Abstract

We introduce a phase field crystal (PFC) model for particles with n-fold rotational symmetry in two dimensions. Our approach is based on a free energy functional that depends on the reduced one-particle density, the strength of the orientation, and the direction of the orientation, where all these order parameters depend on the position. The functional is constructed such that for particles with axial symmetry (i.e. $n = 2$) the PFC model for liquid crystals as introduced by Löwen (2010 *J. Phys.: Condens. Matter* **22** 364105) is recovered. We discuss the stability of the functional and explore phases that occur for $1 \leqslant n \leqslant 6$. In addition to isotropic, nematic, stripe, and triangular order, we also observe cluster crystals with square, rhombic, honeycomb, and even quasicrystalline symmetry. The n-fold symmetry of the particles corresponds to the one that can be realized for colloids with symmetrically arranged patches. We explain how both, repulsive as well as attractive patches, are described in our model.

Keywords: phase field crystal, patchy colloids, free energy functional, anisotropic interaction

(Some figures may appear in colour only in the online journal)

*Author to whom any correspondence should be addressed.

1. Introduction

The formation of patterns in particulate systems is a long-standing topic [1]. A mean field approach to describe the formation of complex equilibrium phases is the so-called phase field crystal (PFC) model [2, 3] where a free energy expansion in a density-like field and its gradient is considered in a way similar as in the well-known approaches by Swift and Hohenberg [4], by Alexander and McTague [5], or by Lifshitz and Petrich [6]. Non-trivial phases are stabilized in PFC models in various ways, e.g., by using more than one length scale [7, 8] (similar as in the Lifshitz–Petrich model [6, 9, 10]) or by introducing a competition with an incommensurate external potential [11, 12]. In another approach anisotropic particles are considered. By introducing an orientational field and couplings between the orientational and the density-like field, PFC models for particles with polar [13] or axial [14–16] symmetry have been modeled. Here we want to generalize these models for particles with other n-fold rotational symmetries. Note, there are other PFC approaches to describe systems composed of particles with a certain rotational symmetry [17, 18]. However, in these approaches the orientation field and the density field cannot vary independently and as a consequence some phases like plastic crystals and oriented crystals cannot be distinguished.

Colloids with a given rotational symmetry can be realized by decorating the particles with attractive or repulsive patches. These so-called patchy colloids are known to exhibit a complex phase behavior [19–24]. Patchy colloids can even be used to obtain quasicrystals [25–28] or to be designed in a way to obtain a complex ordering as desired [29–32].

In this work we want to consider both, attractive and repulsive patches. In case of attractive patches the patches of neighboring particles tend to point towards each other while repulsive patches tend to be oriented away from neighboring patches. As a result neighboring particles either have the same orientation or they are rotated by an angle π/n as illustrated in figure 1.

Note that the particles in this work do not possess any hard core. Therefore, large overlaps can occur and the ordering that we report corresponds to those of so-called cluster crystals [33–36]. Cluster crystals occur naturally in PFC models or related approaches [10] and can form periodic as well as aperiodic structures [10]. In the conclusions in section 4 we will discuss how our approach might be modified in order to describe particles with hard cores, i.e. particles that cannot overlap significantly.

The article is organized as follows: in section 2 we introduce the PFC model for n-fold particles and explain how we determine the stable phases numerically. In section 3 we first present an overview of the phases that occur for various rotational symmetries before we discuss these phases in more detail. Finally, we conclude in section 4.

2. Model

We generalize the PFC models that have been introduced for particles with one-fold [13] or two-fold [14–16] symmetry to particles with n-fold symmetry. We will consider both, attractive and repulsive patches. Concerning the notation, we will follow the model presented in [15], which is shortly outlined in the next subsection.

2.1. Short summary of the PFC model for two-fold symmetry

In [15] Achim *et al* have proposed and studied a PFC model for apolar liquid crystals, i.e. particles of two-fold rotational symmetry. The used free energy functional model had previously

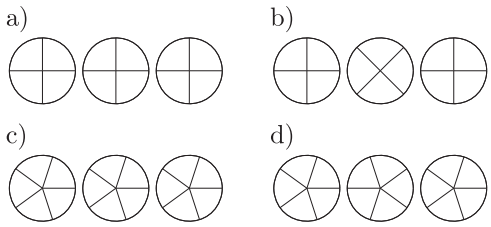

Figure 1. Sketch of the preferred orientation of neighboring particles with (a) and (b) $n = 4$-fold rotational symmetry showing cases that are typical for all even n and (c) and (d) $n = 5$-fold rotational symmetry, which is typical for odd n. In (a) and (c) neighboring particles prefer to possess the same orientation, while in (b) and (d) they prefer alternating orientations, which we realize by a modulated alignment interaction. As a consequence, the cases in (a) and (d) correspond to patchy particles with attractive patches, while in (b) and (c) the patches are repulsive.

been derived by Löwen in [14] from classical density functional theory. The free energy functional therein depends on the one-particle density of a nematic rotator particle that depends on the position $\vec{\mathbf{x}}$ and the orientation ϕ and is approximated as [14]

$$\rho(\vec{x},\phi) \approx \rho_0\left(1 + \psi(\vec{x}) + \frac{1}{2}|U|(\vec{x})\cos(2(\phi - \varphi(\vec{x})))\right) \tag{1}$$

with the density-like field ψ that gives the deviation from the mean density, the nematic order parameter $|U|$, and the nematic director field φ. The free energy functional $\mathcal{F}_{\mathrm{id}}[\rho]$ of the ideal rotator gas is obtained by replacing the density in the well-known free energy of an ideal gas by the density of a rotator particle ρ as given above such that [14]

$$\mathcal{F}_{\mathrm{id}}[\rho] = \frac{1}{\beta}\int \mathrm{d}^2x \int_0^{2\pi} \mathrm{d}\phi\rho\big(\ln\big(\Lambda^2\rho\big) - 1\big) \tag{2}$$

with the inverse temperature β and the thermal wavelength Λ. Using (1) and the expansion

$$(1+x)(\ln(1+x) - 1) = -1 + \frac{1}{2}x^2 - \frac{1}{6}x^3 + \frac{1}{12}x^4 + \mathcal{O}\big(x^5\big), \tag{3}$$

then integrating over the angle and dropping irrelevant constant terms and terms linear in ψ or $|U|$,

$$\mathcal{F}_{\mathrm{id}}\big[\psi,|U|\big] = \int \mathrm{d}^2x\left(\psi^2 - \frac{1}{3}\psi^3 + \frac{1}{6}\psi^4 + \frac{1}{8}|U|^2 + \frac{1}{256}|U|^4 + \frac{1}{8}(\psi-1)\psi|U|^2\right) \tag{4}$$

is obtained as a Landau-like model for the ideal rotator gas [14]. One of these terms, $\frac{1}{8}(\psi-1)\psi|U|^2$, couples ψ and $|U|$. Yet this coupling is isotropic, since it only depends on the intensity, but not the direction of orientation. To consider contributions arising due to interactions between particles, which might also include anisotropic interactions, the expansion of the excess free energy must be considered. As usual for PFC models, a gradient expansion is employed. Again, the details of the expansion are given in [14]. The basic idea is that the excess free energy functional can be given as usual depending on the direct correlation function that is given as function of the positions and orientations of two particles. The terms of the resulting expansion with respect to the density-like field, an orientational field that is further explained below, and the gradients of these fields also depend on the direct

correlation function. As usual for PFC models parameters are used instead of the full dependence on the direct correlation function, though in principle all these dependencies are known (and also given in [14]). As a consequence, the parameters used in the following model are given by the interactions between the particles and can be determined via the direct correlation function.

We now want to introduce the full free energy functional as used in [15], which can be obtained by an expansion [14] as explained before. The functional is based on a complex orientation field that is defined in terms of the nematic order parameter $|U|$ and nematic director field φ as

$$U(\vec{x}) = |U|(\vec{x})\exp(\mathrm{i}2\varphi(\vec{x})). \tag{5}$$

Hence the modulus of U represents the intensity of orientational ordering, while the complex phase encodes the direction. The free energy $\mathcal{F}[\psi, U]$ is given as a functional of the density-like field ψ and the orientation field U. In slightly modified notation, but as studied in [15], the free energy is

$$\begin{aligned}\mathcal{F}[\psi, U] = \int \mathrm{d}^2x \Big(& B_\mathrm{l}\psi^2 + B_\mathrm{x}\psi\big(2\nabla^2 + \nabla^4\big)\psi - \frac{1}{3}\psi^3 + \frac{1}{6}\psi^4 \\ & + D|U|^2 - E\Re\big(U\nabla^2 U^*\big) + \frac{1}{256}|U|^4 \\ & + F\Re\big(U\kappa^2\big)\psi + \frac{1}{8}(\psi - 1)\psi|U|^2\Big)\end{aligned} \tag{6}$$

with the complex derivative operator

$$\kappa = \partial_x - \mathrm{i}\partial_y. \tag{7}$$

The values of the parameters B_l through F are given by generalized moments of the direct correlation function (see above and [14]) and thus can be linked to the temperature, mean density, and the interaction of the modeled particles. They can in principle be determined from measurements of material constants. In the scope of PFC modeling B_l through F can be considered free parameters.

The equilibrium phases are found by minimizing the free energy with respect to the fields ψ and U. Since dynamical processes are not considered in this type of PFC model, different methods for minimization can be chosen, which have often nothing to do with real dynamics. Thus the process of minimization is referred to as *pseudodynamics*. The minima of the free energy are stable or metastable states. In the minimization, the mean of the density-like field is conserved, whereas the orientation field is treated as a non-conserved field. Therefore a suitable choice for pseudodynamical equations reads

$$\frac{\partial\psi}{\partial t} = -\frac{\delta\mathcal{F}}{\delta\psi} + \lambda(t) \tag{8}$$

$$\frac{\partial U}{\partial t} = -\frac{\delta\mathcal{F}}{\delta U^*} \tag{9}$$

with the Lagrange multiplier $\lambda(t)$, keeping the mean of ψ constant. The Lagrange multiplier is not a constant itself, but fluctuates; for details see section 2.3. The density field would as well be conserved, if $\partial\psi/\partial t = \nabla^2\delta\mathcal{F}/\delta\psi$ was applied, instead of (8) [2, 37]. But the numerical treatment of the non-linear terms would be more complicated. Note, we are not aware of any

technique that guarantees that the lowest energy has been found and real dynamics can also get stuck in metastable states. As usual, by using different candidate structures and random initial states and by comparing the free energies of the observed minima, one at least can identify the lowest energy that can be reached from the initializations.

Before generalizing the free energy for particles with n-fold symmetry, we shortly discuss the roles of the parameters and the terms that are obtained from an expansion of the excess free energy and thus are not just given by the ideal rotator gas (see also discussion in [15]). The value of $B_\mathrm{l} - B_\mathrm{x}$ determines whether modulations in density are energetically favorable. In reciprocal space the respective contributions are $\left(B_\mathrm{l} + B_\mathrm{x}\left(-2k^2 + k^4\right)\right)|\mathfrak{F}\psi|^2$, where $\mathfrak{F}$ denotes the Fourier transformation. This expression has a minimum at $k = 1$, where its value is $(B_\mathrm{l} - B_\mathrm{x})|\mathfrak{F}\psi|^2$. Therefore density modulations of wave number $k = 1$ decrease the free energy if $B_\mathrm{l} - B_\mathrm{x} < 0$, while modulations with other wavelengths are less favorable which can be attributed to the elasticity of the system. For small values of D, strong nematic order is favored, whereas nematic order vanishes for large D. Around $D = 0$ crystalline phases with non-vanishing nematic order are observed [15]. Thus D is related to the orientational interactions between particles, i.e. it denotes how strongly particles want to align with neighboring particles. The term proportional to E (E-term) can be rewritten via integration by parts in the form $E\nabla U \cdot \nabla U^*$. Hence it is a diffusion term, suppressing modulations in the orientation field and ensuring stability for $E > 0$. The F-term is the lowest-order anisotropic coupling between ψ and U. Thus it denotes that a density gradient might change the orientation or vice versa. It is the simplest term that couples the density and the direction of orientation, while respecting two-fold rotational symmetry. Since the sign of U does not enter any of the other terms, the free energy is invariant under a sign change of F and U. Thus only values $F \geqslant 0$ need to be considered [15]. For $F = 0$ the phases with modulated density have vanishing orientations and the nematic phase is the only phase that shows a finite orientation, while for $F > 0$ new phases with non-vanishing orientations are obtained [15].

2.2. New generalization for n-fold symmetry

We now want to generalize the free energy functional of (6) to n-fold symmetry. First, the definition of the orientation field from (5) is generalized to

$$U(\vec{x}) = |U|(\vec{x})\exp(\mathrm{i}n\varphi(\vec{x})). \tag{10}$$

In this way the interpretation of U is compatible with n-fold symmetry, since the complex phase of U is $2\pi/n$-periodic in the director field φ. This means U performs a full turn in the complex plane when the particle orientation rotates by $2\pi/n$.

Note that the F-term in (6) is the only contribution to the free energy that depends on the complex phase of U. Since all terms in $\mathcal{F}[\psi, U]$ need to be invariant under local rotations of the coordinate system, the F-term needs to be adjusted to the new definition of U. The operator κ transforms under a local rotation of the coordinate system by an angle α as $\kappa' = \kappa\,\mathrm{e}^{-\mathrm{i}\alpha}$. Therefore, $U\kappa^n$ is the simplest term that is linear in U and that respects local n-fold rotational symmetry. Hence the F-term of (6) is generalized to

$$F\Re(U\kappa^n)\psi. \tag{11}$$

A modification of the E-term proves to be necessary for numerical stability as we will explain in more detail in our discussion of the stability presented in section 3.1. Hence we replace the operator $-\nabla^2$ in the E-term by $f\left(\nabla^2\right)$. Moreover, this generalization permits

Table 1. Comparison of terms occurring in the excess free energy for polar (one-fold) particles [13], including nematic (two-fold) contributions, with the respective terms for purely two-fold [14] and one-fold symmetry. The single terms are referenced by their coefficients in the notation of the respective publication. Terms that cannot occur in a model are marked with a dash (—) and deviations are specified. The terms of [13], proportional to E_1 through G_7, are unparalleled in [14] and this work. Moreover the terms in [15] are identical to those in [14], up to a rescaling, which merges B and C of [14] into B_x of [15].

$n=2$ [14]	$n=1\,\&\,2$ [13]	$n=1$ (this work)
A	A_1	B_l
B	A_2	$\}B_\mathrm{x}$
C	A_3	
—	B_1	F, up to an irrelevant sign
—	B_2	—
F, lacking contributions of $\nabla\varphi$	B_3	—
—	C_1	D
—	C_2	E, up to modifications
—	C_3	Lacking
D	D_1	—
E	D_2	—

modulated alignment that will be used to reflect both repulsive as well as attractive patches as will be explained in section 2.4.

With the E-term and F-term modified, the free energy becomes

$$\begin{aligned}\mathcal{F}[\psi,U]=\int \mathrm{d}^2x\,\Big(&B_\mathrm{l}\psi^2+B_\mathrm{x}\psi\big(2\nabla^2+\nabla^4\big)\psi-\frac{1}{3}\psi^3+\frac{1}{6}\psi^4\\&+D|U|^2+E\Re\big(Uf\big(\nabla^2\big)U^*\big)+\frac{1}{256}|U|^4\\&+F\Re(U\kappa^n)\psi+\frac{1}{8}(\psi-1)\psi|U|^2\Big).\end{aligned}\tag{12}$$

This is the new free energy functional for particles with n-fold rotational symmetry that we study in this article.

When keeping $f\big(\nabla^2\big)=-\nabla^2$ and specializing to $n=2$, our model reduces to the one from [15]. Moreover, the generalization proposed here is in accordance with a model for polar liquid crystals, i.e. particles of one-fold rotational symmetry ($n=1$), presented by Wittkowski *et al* in [13]: for example, the F-term for $n=1$ can be identified with the term proportional to B_1 in [13]. Table 1 provides a detailed comparison of all terms. Note that although [13] considers polar particles of one-fold symmetry, contributions of two-fold (nematic) symmetry are taken into account in [13], by introducing fields for both, polar and nematic order parameter. This is reasonable, since the two-fold symmetry is compatible with the underlying one-fold symmetry. The two-fold contributions can thus be seen as an extension upon the lowest-order orientational ordering. Yet, the number of parameters is drastically increased due to the multitude of cross terms. We narrow down the number of terms in the free energy functional by restriction to a single orientation field, representing the fundamental contribution of n-fold symmetry.

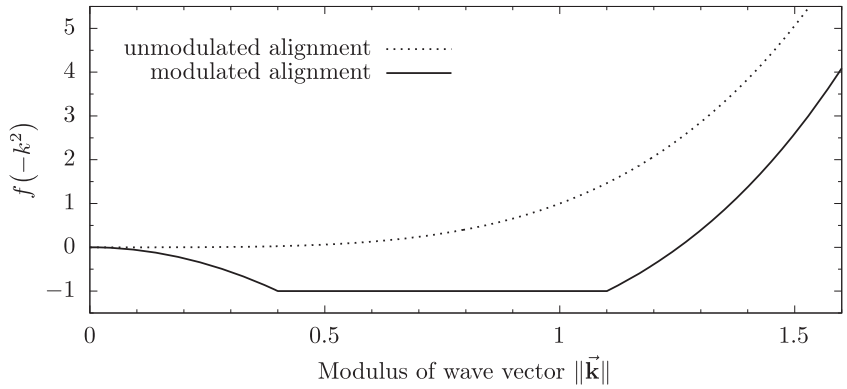

Figure 2. The functions $f\left(-k^2\right)$ as defined for unmodulated alignment in (17) and piecewise defined for modulated alignment in (18), both here with $m = 4$.

2.3. Minimization scheme and numerical details

Motivated by the numerical investigation of systems with axial symmetry by Achim *et al* [15] we implement a similar combination of explicit Euler integration in direct space for the contributions from $\mathcal{F}_{\text{dir}}$ and implicit Euler integration in reciprocal space for the contributions from $\mathcal{F}_{\text{rec}}$. Conveniently, the terms of $\mathcal{F}[\psi, U]$, that are quadratic or bilinear in ψ or U, can be expressed in reciprocal space, where spatial derivation reduces to multiplication with wave vector components. Since the functional derivatives of quadratic or bilinear expressions lead to linear terms in the differential equation, implicit Euler integration can be performed on these terms to improve numerical stability.

To be specific, the explicit Euler integration in direct space is given by

$$\psi' = \psi - \Delta t \frac{\delta \mathcal{F}_{\text{dir}}}{\delta \psi}[\psi, \Re U, \Im U], \tag{13}$$

$$\Re U' = \Re U - \Delta t \frac{\delta \mathcal{F}_{\text{dir}}}{\delta \Re U}[\psi, \Re U, \Im U], \tag{14}$$

$$\Im U' = \Im U - \Delta t \frac{\delta \mathcal{F}_{\text{dir}}}{\delta \Im U}[\psi, \Re U, \Im U] \tag{15}$$

and the implicit Euler integration in reciprocal space leads to an evolution according to

$$\begin{pmatrix} \mathfrak{F}\psi'' \\ \mathfrak{F}\Re U'' \\ \mathfrak{F}\Im U'' \end{pmatrix} = (1 - \Delta t L)^{-1} \begin{pmatrix} \mathfrak{F}\psi' \\ \mathfrak{F}\Re U' \\ \mathfrak{F}\Im U' \end{pmatrix} \tag{16}$$

where $\mathfrak{F}$ denotes the Fourier transformation and L is a matrix that contains coefficients stemming from the functional derivatives of $\mathcal{F}_{\text{rec}}$. The terms in the matrix L will be shortly discussed in the stability analysis in section 3.1 and the functional derivatives are given in the appendix A. After the implicit integration, the Lagrange multiplier is applied, setting the appropriate value for the $\vec{\mathbf{k}} = 0$-component of $\mathfrak{F}\psi''$. The backwards transformation to direct space completes the timestep.

We apply periodic boundary conditions and discretize ψ and U on a grid of 512×512 or 1024×1024 points. The intrinsic lengthscale is set by the B_{x}-term to $k = 1$, i.e. a

peak–peak distance of 2π in direct space. The system size spans 10 to 14 peak–peak distances, such that single peaks, as well as structures much larger than the typical unit cell are resolved. We perform several computations for each point in phase space, starting from random noise in both fields. When the resulting free energies differ, which happens when defects or metastable structures appear, we start more computations with appropriately patterned initial fields. The structure that yields the lowest free energy is assumed to be the equilibrium phase.

2.4. Modulated or unmodulated alignment to implement attractive or repulsive patches

Here we explain how the function $f\left(\nabla^2\right)$ (or $f\left(-k^2\right)$ in reciprocal space) is chosen such that either the alignment or the anti-alignment of neighboring particles is preferred. Note that the differences in alignment of neighboring particles is used to model repulsive or attractive patches as sketched and explained in figure 1. The asymptotics of $f\left(-k^2\right)$, i.e. the behavior at large wave vectors, are dictated by the stability requirement which will be discussed in section 3.1.

In case neighboring particles prefer to align, we use a monotonic function namely

$$f\left(-k^2\right) = k^m \tag{17}$$

with $m = \max\{2n-4, 2\}$. Note that for $n = 2$ the term used in [15] is obtained.

In case the anti-alignment of neighboring particles is preferred, the function $f\left(-k^2\right)$ should be non-monotonic, leading to a negative free energy contribution for an orientation that alternates on the length given by the nearest neighbor distance. As anti-aligned particles experience a rotation of π/n from one particle to its neighbor, the period of U amounts to two particle distances. This corresponds to a wavelength of $k = \frac{1}{2}$. Hence $f\left(-k^2\right)$ should have a minimum at $k = \frac{1}{2}$. However, we aim not to introduce a second lengthscale via the preferred wavelength of alignment. Thus we choose a broad minimum in $f\left(-k^2\right)$, extending beyond $k = \frac{1}{2}$ and $k = 1$. Furthermore, the asymptotics should be similar as for the alignment case to ensure stability. Based on these requirements we employ a continuous piecewise-defined term namely

$$f\left(-k^2\right) = \begin{cases} -\left(k/0.4\right)^2 & \text{for } k^2 \leqslant 0.4^2 \\ -1 & \text{for } 0.4^2 < k^2 \leqslant 1.1^2 \\ k^m - 1.1^m - 1 & \text{for } 1.1^2 < k^2. \end{cases} \tag{18}$$

We call this case the modulated alignment case. The first piece of this function leads to a continuous connection from $f(0) = 0$ to $f\left(-0.4^2\right) = -1$. The $k = 0$-component of the orientation field is the global orientational order, which is already controlled by the parameter D. By choosing $f(0) = 0$, D has the same meaning for modulated and unmodulated alignment and is not shifted by E under modulated alignment. The second piece of the function is the extended minimum and the third piece ensures stability by suppressing short-length modulations in the orientation field, with $m = \max\{2n-4, 2\}$ as before. For both types of alignment the functions are depicted in figure 2.

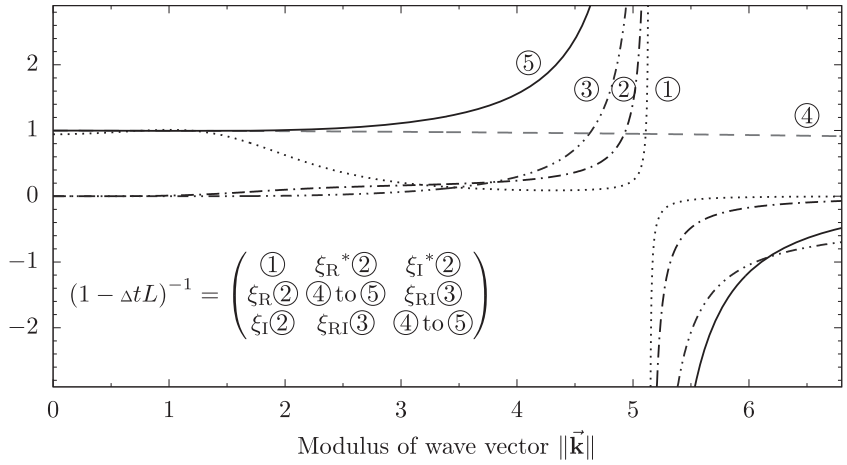

Figure 3. Matrix elements from (19) as functions of the wave vector. Plotted are the most extreme contours, which are observed along certain radial directions in reciprocal space. The diagonal elements vary between functions ④ and ⑤, depending on direction. The factors ξ_R, ξ_I, ξ_{RI} arise from the real and imaginary part of κ^n. They are $2\pi/n$-periodic in the polar angle associated with direction of the wave vector. ξ_{RI} ranges from -1 to 1; both, ξ_R and ξ_I, range from -1 to 1 for even n and from $-\mathrm{i}$ to i for odd n, respectively. Parameter values are $\Delta t = 1 \times 10^{-2}$, $B_l = 3.0$, $B_x = 3.5$, $D = 0.1$, $E = 0.1$, $F = 1.0$, $f\left(\nabla^2\right) = -\nabla^2$, and $n = 4$.

3. Results

3.1. Stability requirement

To study the stability we have a closer look at the implicit integration step (16) that corresponds to the linear contribution of the integration and is governed by a matrix

$$(1-\Delta tL)^{-1} = \frac{1}{ad - |c_R|^2 - |c_I|^2}\begin{pmatrix} d & -c_R{}^* & c_I{}^* \\ -c_R & a - |c_I|^2/d & -c_R c_I{}^*/d \\ c_I & -c_R{}^* c_I/d & a - |c_R|^2/d \end{pmatrix} \tag{19}$$

with

$$a = 1 + 2\Delta t(B_l + B_x(-2k^2 + k^4)) \tag{20}$$

$$c_R = \Delta t F \mathrm{i}^n \Re\left(\left(k_x - \mathrm{i}k_y\right)^n\right) \tag{21}$$

$$c_I = -\Delta t F \mathrm{i}^n \Im\left(\left(k_x - \mathrm{i}k_y\right)^n\right) \tag{22}$$

$$d = 1 + 2\Delta t(D + Ef(-k^2)). \tag{23}$$

See the appendix A for how this matrix is obtained from the free energy functional. We now want to choose $f\left(\nabla^2\right)$ such that the integration is stable. Note that in general the choice that is used in [14, 15] is not suitable: for example, if $n \geqslant 4$ and the E-term was given by $f\left(\nabla^2\right) = -\nabla^2$, the computations would exhibit a numerical instability for many (significant) regions in physical parameter space.

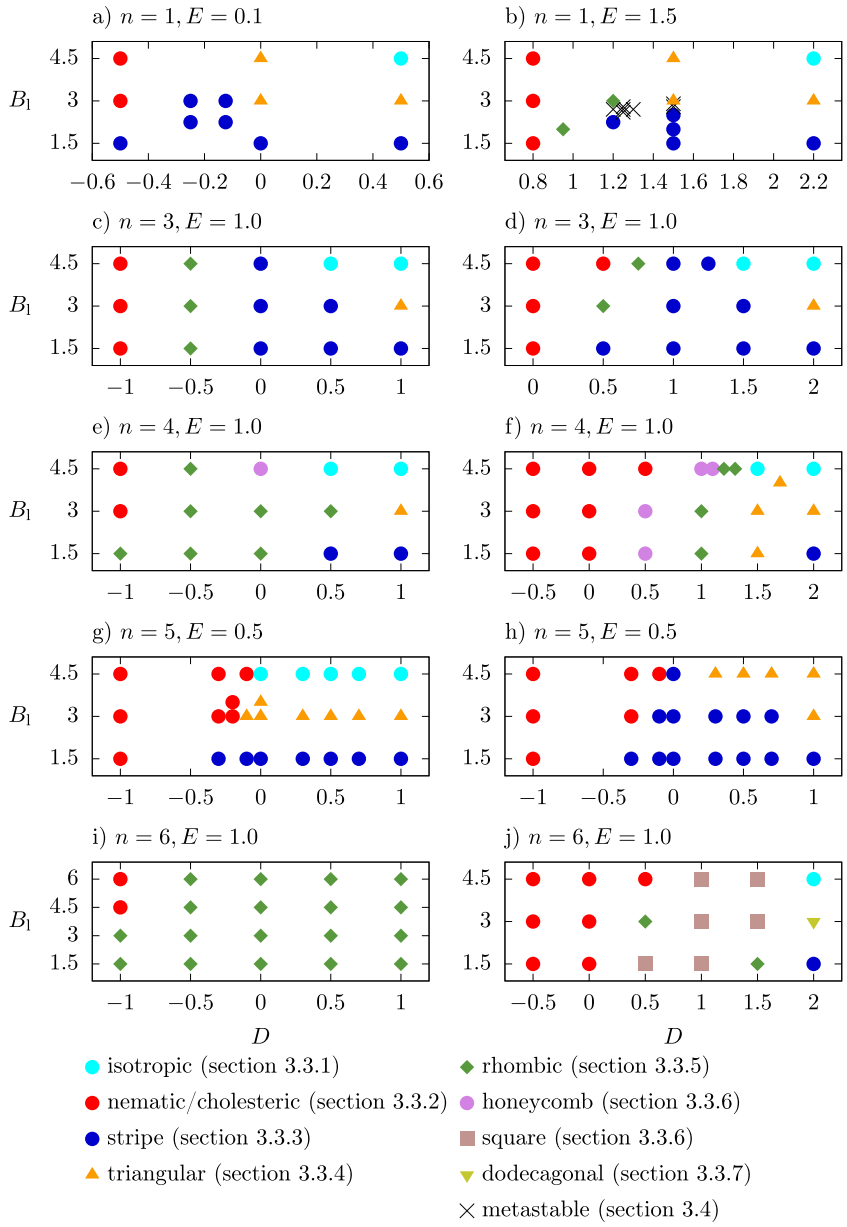

Figure 4. Left column: unmodulated, right column: modulated alignment. $F = 0$ gives only isotropic, triangular, stripe with vanishing U, and nematic or cholesteric phase. We choose standard parameters $B_x = 3.5, F = 1.0$ and $E = 0.1$ for unmodulated alignment and $E = 1.0$ for modulated alignment, respectively. We have tried combinations of these values and $B_x = 1.0, E = 3.5, F = 3.0$, without finding different phases.

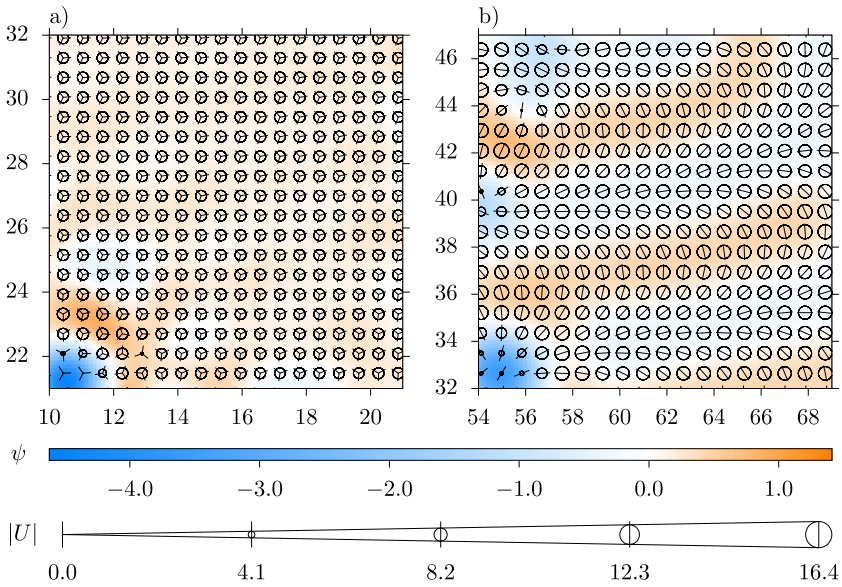

Figure 5. Phases that occur for small D, where the orientational field is strong. (a) Nematic phase for unmodulated alignment and $n = 3, B_\mathrm{l} = 3.0, B_\mathrm{x} = 3.5, D = -1.0, E = 0.1, F = 1.0$. (b) Cholesteric phase for modulated alignment and $n = 2, B_\mathrm{l} = 1.5, B_\mathrm{x} = 3.5, D = -1.0, E = 0.4, F = 1.0$. In equilibrium the density in the nematic phase is constant while the cholesteric phase possesses stripe-like density modulations. Large variations in density only appear in case of topological defects in the director field as depicted here in the lower left parts of the figures.

In figure 3 we plot the matrix elements of (19) as functions of $\vec{\mathbf{k}}$. All of the matrix elements have poles at certain values of $\vec{\mathbf{k}}$. These poles derive from a root of the determinant of $1 - \Delta t L$, which enters into (19) as denominator. The position of the poles depends on the physical parameters of the free energy functional and also on the timestep Δt of Euler integration. For sufficiently small Δt, the poles fall outside the range of numerically accessible wave vectors. Hence Δt can be chosen small enough to avoid numerical instability caused by the poles themselves.

Yet a different cause of instability remains, independent of Δt: in certain directions in reciprocal space the diagonal elements that correspond to the curves labeled by ⑤ in figure 3 exceed 1 for all wave vectors up to the pole. These matrix elements let the high-frequency modes grow, while the terms in $\mathcal{F}_\mathrm{dir}$ of higher order in ψ and U either overcompensate or fail to compensate for this growth.

To guarantee stability we want the respective matrix elements to fall below 1, i.e.

$$1 \geqslant \frac{a}{ad - |c_\mathrm{R}|^2 - |c_\mathrm{I}|^2} \quad \Leftrightarrow \quad F^2 \leqslant \frac{a(d-1)}{\Delta t^2 k^{2n}}. \tag{24}$$

This relation can be used to compute the maximum F, for which the calculations will be stable, given the timestep Δt, the maximum length of contributing wave vectors k, and the parameters of the free energy functional. In addition, the relation (24) permits us to pinpoint a condition on the asymptotics of the E-term, necessary for numerical stability at arbitrary non-zero F. Let $f\left(-k^2\right)$ be of order $\mathcal{O}(k^m)$ for large wave vectors $k \gg 1$. Then (24) is

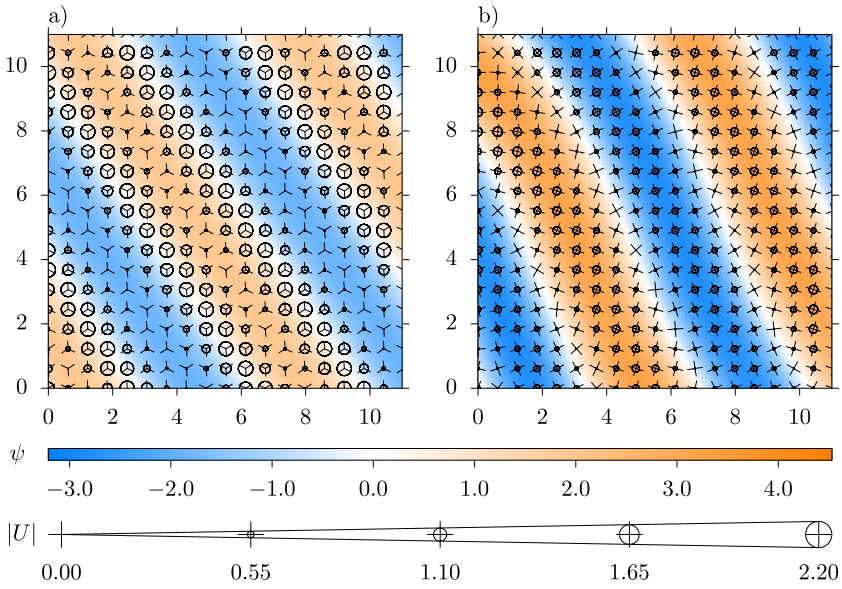

Figure 6. Typical stripe phases as they occur e.g., for (a) unmodulated alignment and $n = 3, B_\mathrm{l} = 3.0, B_\mathrm{x} = 3.5, D = 0.5, E = 0.1, F = 1.0$ and (b) modulated alignment and $n = 4, B_\mathrm{l} = 1.5, B_\mathrm{x} = 3.5, D = 2.0, E = 1.0, F = 1.0$. The orientation fields of the stripe phases depend only on n and are independent of (un)modulated alignment.

expressed as

$$F^2 \leqslant \frac{4}{\Delta t^2} B_\mathrm{x} E k^{4-2n} f\left(-k^2\right) + \mathcal{O}\left(k^{m-2n+3}\right). \tag{25}$$

In order to ensure that this relation holds for a finite F and arbitrarily large k, $m \geqslant 2n-4$ is required. Conversely the function in the E-term has to behave asymptotically like

$$f\left(-k^2\right) \propto k^{2n-4} \quad \text{for } k \gg 1 \tag{26}$$

or like a term of higher order in k. Only then the right-hand side expression of (25) does not tend to zero for large k.

If we considered conserved dynamics with a Laplacian instead of the negative gradient that we use in our pseudodynamical equation (8), some of the matrix elements would change. However, the position of the pole and the problem of matrix elements exceeding 1 up to the pole would remain unchanged and we would obtain the same stability criterion.

Note that qualitatively the order of the term $f\left(-k^2\right)$ seems not to matter as long as the integration is stable. For example, for liquid crystals ($n = 2$) we have found the same phases as in [15] even if we use $f\left(-k^2\right) = k^4$ instead of $f\left(-k^2\right) = k^2$.

3.2. Overview of the phase behavior

Due to the number of parameters and the rich zoo of complex phases that can occur, systematic studies of the whole parameter space are difficult. Our goal in this work is not to present complete phase diagrams. In this and the following subsections we want to present typical phases that can occur in systems for various rotational symmetries. Concerning the parameters

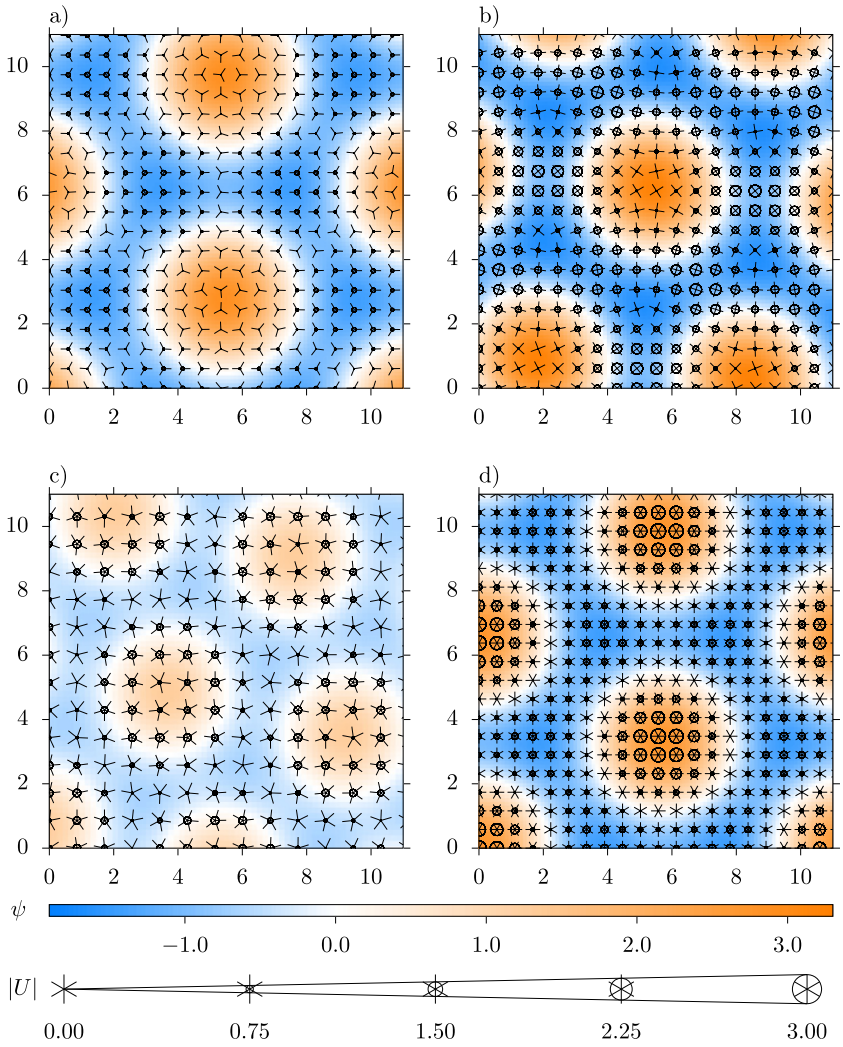

Figure 7. Triangular phases for (a) unmodulated alignment and $n = 3, B_l = 3.0, B_x = 3.5, D = 1.0, E = 0.1, F = 1.0$, (b) modulated alignment and $n = 4, B_l = 3.0, B_x = 3.5, D = 1.5, E = 1.0, F = 1.0$, (c) modulated alignment and $n = 5, B_l = 4.5, B_x = 3.5, D = 1.0, E = 0.5, F = 1.0$, and (d) modulated alignment and $n = 6, B_l = 3.0, B_x = 3.5, D = 1.0, E = 1.0, F = 1.0$. In (d) $|U|$ is twice as large as plotted and the phase is metastable.

we have focused on the regions in parameter space where non-trivial phases are expected as discussed e.g., in the work by Achim *et al* on two-fold particles [15].

In figure 4 we show an overview of the phases that we have found in systems with $1 \leqslant n \leqslant 6$ both, for alignment between neighboring particles (left column in figure 4) as well as modulated alignments (right column). While the figures shown in figure 4 not necessarily are complete phase diagrams as we cannot be sure whether there are additional intermediate phases (see also discussion in section 3.4), the figures demonstrate the typical phases that occur in the small and large limits of D for almost all rotational symmetries namely a nematic or

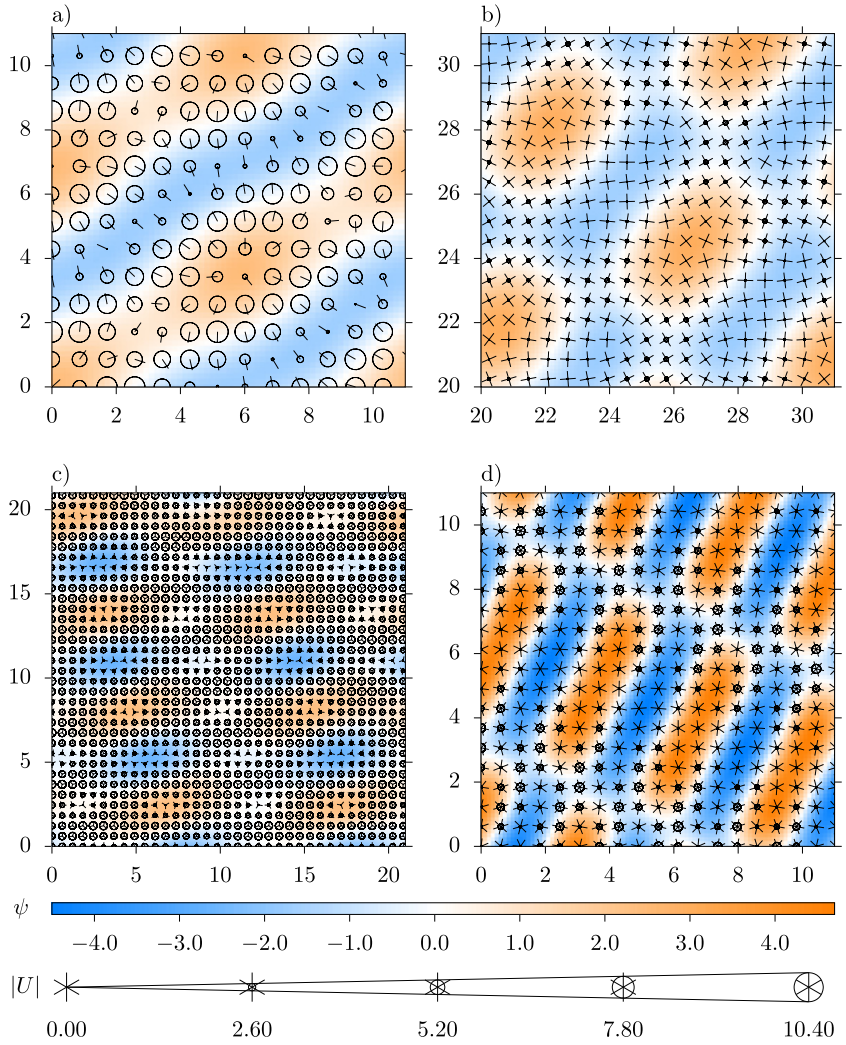

Figure 8. Rhombic phases for (a) modulated alignment and $n = 1, B_l = 2.0, B_x = 3.5, D = 0.95, E = 1.5, F = 1.0$, (b) unmodulated alignment and $n = 4, B_l = 3.0, B_x = 3.5, D = 0.5, E = 1.0, F = 1.0$, (c) modulated alignment and $n = 5, B_l = 4.5, B_x = 3.5, D = 0.5, E = 1.0, F = 1.0$, and (d) unmodulated alignment and $n = 6, B_l = 6.0, B_x = 3.5, D = 0.5, E = 0.1, F = 1.0$.

cholesteric phase for small D and usually stripe, triangular, and isotropic phases for large D. Furthermore, in the overviews some non-trivial phases that occur in between are shown. Details of the phases are discussed in the following subsections as denoted in the legend of figure 4.

3.3. Discussion of stable phases

In the following we discuss the stable phases that we observe in detail.

Note that in all snapshots depicting the phases the color denotes the density-like field $\psi(\mathbf{x})$. The orientation field $U(\mathbf{x})$ is superimposed over ψ in the form of markers, which show the

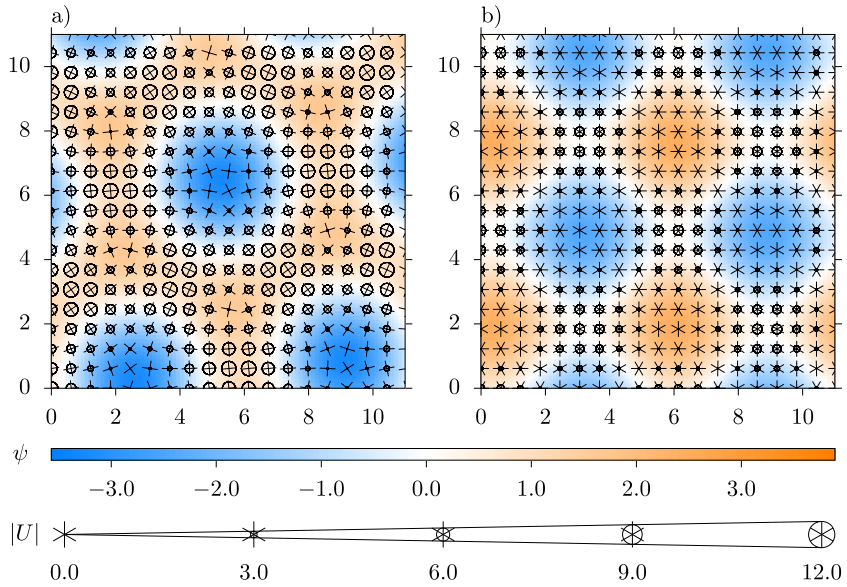

Figure 9. (a) Honeycomb phase for modulated alignment and $n = 4, B_\mathrm{l} = 3.0, B_\mathrm{x} = 3.5, D = 0.5, E = 1.0, F = 1.0$ and (b) square phase for modulated alignment and $n = 6, B_\mathrm{l} = 4.5, B_\mathrm{x} = 3.5, D = 1.0, E = 1.0, F = 1.0$.

symmetry and direction. Furthermore, the size of the circle at the markers denotes magnitude $|U|$. Note that the fields U and ψ are determined with the same spatial resolution. However, we plot fewer orientation markers to keep the plots legible.

3.3.1. Isotropic phase. For large D and large B_l an isotropic phase is observed. In the isotropic phase the density is homogeneous and the magnitude $|U|$ of the orientation field vanishes, i.e., there is no preferred orientation of the particles.

3.3.2. Nematic and cholesteric phases. For small D structures with strong orientational order occur. In case neighboring particles prefer to align, i.e. for unmodulated interactions, a nematic phase is found as depicted in figure 5(a). If neighboring particles prefer opposite orientations, i.e. for modulated alignment interactions, we observe a phase where a strong orientation changes continuously in a wave-like pattern. We call this structure a cholesteric phase.

While in an ideal nematic phase all particles possess the same orientation, in the cholesteric phase particles with similar orientation occur along stripes. Furthermore, the density is constant in the nematic phase but there is a stripe-like weak density modulation in the cholesteric phase.

In both phases, when defects are present, they tend to cluster in motifs that occur in close-by phases.

3.3.3. Stripe phases. For small B_l and usually larger D stripe phases with a strongly modulated density occur. The stripe phases of modulated and unmodulated alignment are identical. For all odd n we observe the strongest modulations to appear where the density gradient is maximal as depicted in figure 6(a). In contrast, for all even n, figure 6(b), the orientational

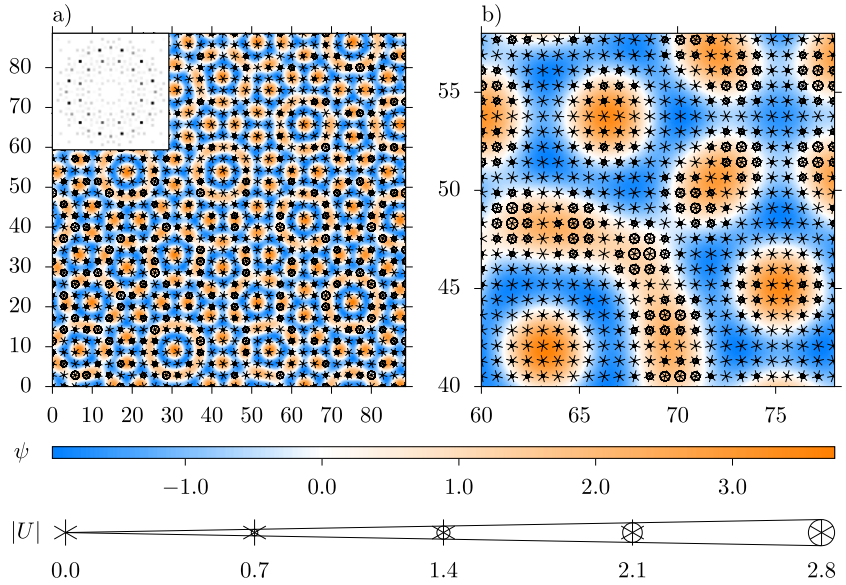

Figure 10. Dodecagonal quasicrystal for modulated alignment and $n = 6, B_l = 3.0, B_x = 3.5, D = 2.0, E = 1.0, F = 1.0$. The inset shows the Fourier transform of ψ and (b) is a zoom-in on the configuration from (a).

strength is maximal in the density maximum as well as in opposite direction (rotated by π/n) in the density minimum but vanishes at the flanks of the stripes.

3.3.4. Triangular phases. The triangular phases occur at larger B_l than the stripe phases. Similar to the stripe phases, the orientation fields of the triangular phases depend whether n is even or odd; yet with exceptions when n matches a symmetry of the triangular lattice. Typically for even n the orientation is strong between neighboring density peaks, see figure 7(b), while for odd n each density peak is surrounded by a ring of strong orientation as shown in figure 7(c). In both cases the orientation vanishes at the density maxima, marking the triangular phases as plastic crystals. Exceptions of this general rule are $n = 3$ and $n = 6$: figure 7(a) shows the triangular phase of $n = 3$, exhibiting strong orientation not between pairs, but between triplets of neighboring density peaks. Figure 7(d) presents the triangular phase of $n = 6$, which is an oriented crystal. However, it only occurs as metastable phase as the dodecagonal quasicrystal is stable for these parameters.

3.3.5. Rhombic phases. Figure 8 shows several rhombic phases for different n. The rhombic phases often appear at intermediate D between the nematic or cholesteric phase and other crystalline phases. In some cases the angles that occur might not be uniquely given: for modulated alignment next to the cholesteric phase, the rhombic phase often can be stretched or compressed at almost no energy cost, because there is a flat segment in the piecewise definition of $f\left(-k^2\right)$ in (18).

3.3.6. Honeycomb and square phases. The honeycomb and square phases, depicted in figure 9, add to the examples of plastic crystalline phases which appear in between the ubiquitous phases. Their topology is the same as reported for two-fold particles in [15]. Surprisingly,

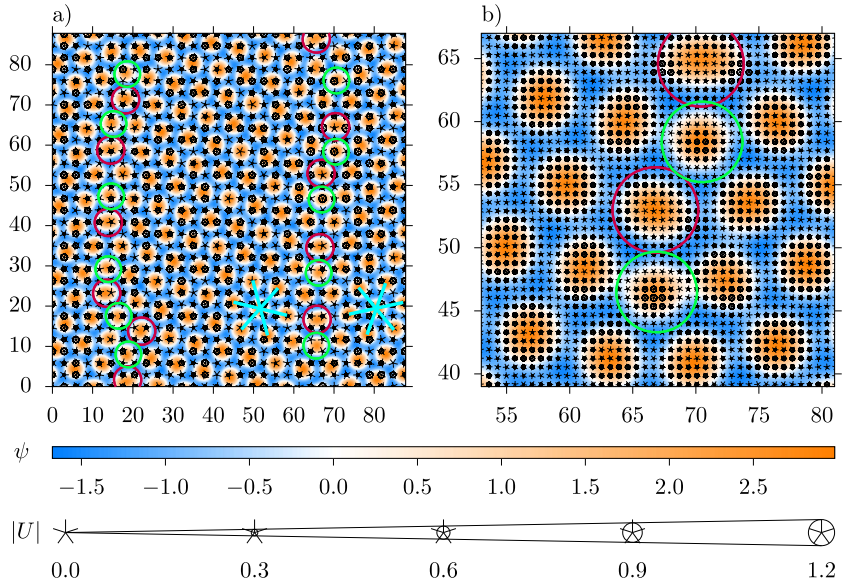

Figure 11. Defects along a grain boundary of the triangular phase of five-fold particles for unmodulated alignment and $B_\mathrm{l} = 3.0, B_\mathrm{x} = 3.5, D = 0.7, E = 0.5, F = 1.0$. The stable phase for these parameters is a triangular crystal. The orientations of the two grains are highlighted in cyan, seven-neighbor dislocations are marked in purple, and five-neighbor dislocations in green. The orientation field is large on the density peaks with five neighbors, as shown in (b), a zoom-in on the configuration from (a).

the honeycomb phase is stable for four-fold particles and the square phase is stable for six-fold particles, but not vice versa. This underlines again, like the rhombic phases, that the symmetry of the particles does not dictate the symmetry of the emergent crystal.

3.3.7. Dodecagonal quasicrystalline phase. We also find a stable quasicrystal, i.e. a structure with long-ranged order but without translational symmetry. The observed quasicrystal is shown in figure 10. It possesses twelve-fold rotational symmetry and occurs for a system with modulated alignments and particles with six-fold rotational symmetry. From a zoom-in to the quasicrystalline structure as shown in figure 10(b) one recognizes that along a ring around a local symmetry center there are 12 regions with strong orientation. The orientation in neighboring regions is rotated by $\pi/6$ as expected due to the modulation of the alignment interaction. Probably these regions are the features that stabilize the quasicrystals.

As typical to quasicrystals, the Fourier transform of ψ exhibits not only the 12 main peaks but numerous quite strong satellite peaks as well. Therefore, the anisotropic interaction can indeed lead to the stabilization of lengthscales that differ from the length that is preferred by the free energy functional.

In principle a similar structure might occur for particles with twelve-fold rotational symmetry and unmodulated alignment interactions. However, we have not found such a quasicrystal. Furthermore, we have not observed any stable quasicrystals with other rotational symmetry.

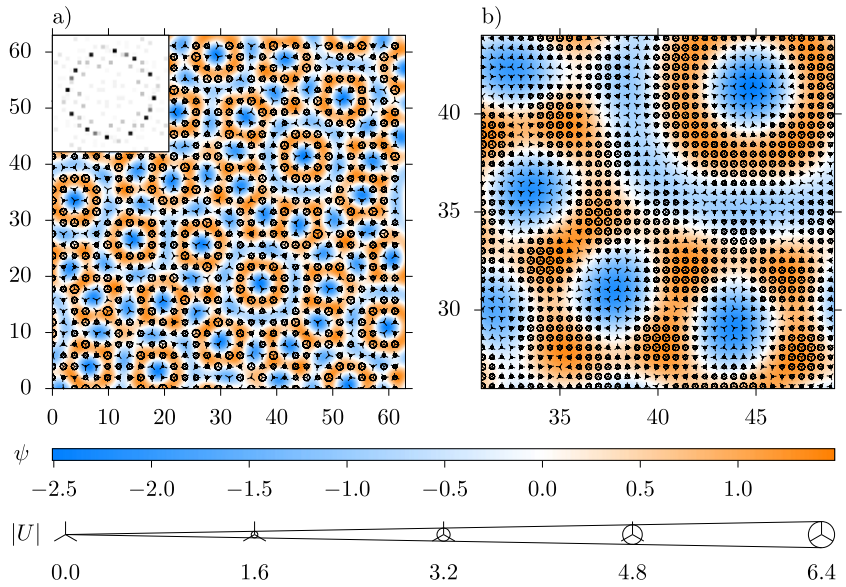

Figure 12. Metastable dodecagonal quasicrystal for modulated alignment and $n = 3, B_l = 4.5, B_x = 3.5, D = 1.0, E = 1.0, F = 1.0$. Note that the stable phase for these parameters is the stripe phase. The inset shows the Fourier transform of ψ and (b) is a zoom-in on the configuration from (a).

3.4. Defects and metastable states

Although we do not observe any stable quasicrystals composed of particles with five-fold rotational symmetry, it seems that five-fold symmetry prominently occurs in defects along grain boundaries as shown in figure 11. The grain boundaries contain the well known pairs of dislocations with five and seven neighbors [38]. Yet the density peaks with five neighbors stand out, as the orientation field on the peaks is large, whereas it vanishes on the peaks with six or seven neighbors.

We also observe metastable quasicrystals like the one shown in figure 12 that are different from the dodecagonal structure reported in section 3.3.7. The stabilization mechanism for the three-fold particles is probably the same as for the six-fold ones, where the orientation field modulates along the rings of high density. Despite having the same 12-fold symmetry, the metastable quasicrystal consists almost entirely of rings of high density and very few isolated density peaks, as opposed to the stable quasicrystal. Moreover the satellite peaks of this structure in reciprocal space are much less pronounced. In this case the stripe phase is stable, i.e. has a lower free energy than the metastable quasicrystal.

The figures shown in figure 4 are not necessarily complete phase diagrams. In some cases it is hard to figure out whether a resulting structure is stable or metastable. For example in figure 4(b) some points in parameter space are marked with crosses. For these parameters we observe structures that seem to be mixtures of triangular, stripe, and possibly rhombic phase as shown in figure 13. Note that the corresponding pure phases possess a higher free energy than the mixture that we observe. Probably in these points the true equilibrium phase has not been found yet.

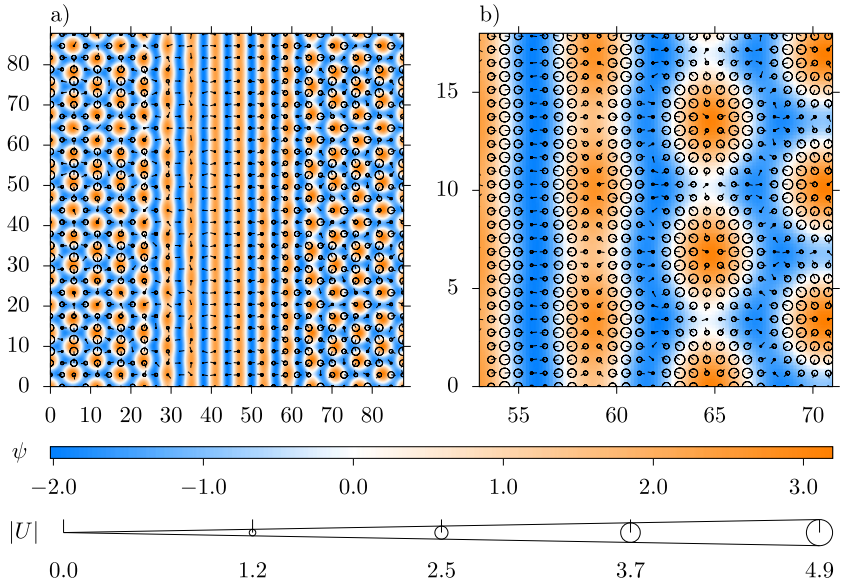

Figure 13. Mixture of triangular, stripe, and possibly rhombic phase for modulated alignment and $n = 1, B_l = 2.9, B_x = 3.5, D = 1.5, E = 1.5, F = 1.0$. (b) Is a zoom-in on the configuration from (a).

4. Conclusions

We have introduced a new PFC model for particles with n-fold rotational symmetry in two dimensions as it occurs, e.g., for patchy particles with symmetrically placed patches. Both the cases of attractive as well as repulsive patches have been considered leading either to alternating or the same orientation of neighboring clusters.

The PFC model is used to determine the phases that are stable for various rotational symmetries. We usually observe nematic or cholesteric phases in case a non-vanishing orientational order is preferred by the free energy. In the opposite limit we find stripe, triangular, or isotropic phases depending on how strong density modulations are supported. In between these phases, complex orderings with honeycomb, square, or rhombic symmetry occur. We even find a quasicrystalline phase with dodecagonal rotational symmetry. Therefore it is demonstrated that quasicrystals can be stabilized by interactions that only possess one length scale if in addition special binding angles are preferred. Note that we do not find the type of quasicrystals that has been reported to occur for patchy particles in simulations [25–28]. As we will discuss in the last paragraph this is probably due to lack of a hard core in our approach.

Since a lot of complex phases occur in our system, finding the global minimum might be hard and usually there are a lot of metastable states with interesting structures. At the end of section 3 we shortly comment on some examples including a metastable quasicrystal. However, the metastable states deserve more detailed analyses in future works. For example, the domains that meet at grain boundaries prefer orientations that depend on the rotational symmetry and the orientational interactions. As a consequence the grain boundaries probably differ

from the boundaries that are observed for isotropic particles. By adding noise the coarsening processes in systems with such grain boundaries can be explored, which we leave for future works.

The particles that we have in mind in this work do not possess a hard core. Therefore, the phases described here correspond to cluster crystals similar as in [10, 33–36, 39]. In contrast, in many particulate systems a hard core prevents large overlaps of particles. Furthermore, a hard core can support the formation of some complex phases like quasicrystals [40–42]. Note that the quasicrystalline phases that have been observed in computer simulations of patchy colloids have been found in systems where the particles can hardly overlap [25–28]. As a consequence, in future we want to study mean field approaches with similar couplings between an orientational field and the density-like field as in this article. However, to model a hard core as well, the functional dependence on the density-like field has to be changed. A suitable way to describe the hard core is given by the so-called fundamental measure theory [43–45], which can be formulated in two dimensions [46] and which is known to lead to complex phases in case of the competition with an incommensurate substrate [47–49].

Acknowledgments

This work is supported by the Deutsche Forschungsgemeinschaft (Grant SCHM 2657/4-1).

Data availability statement

The data that support the findings of this study are available upon reasonable request from the authors.

Appendix A

For the following calculations we introduce the shorthand notation $p = \Re U$ and $q = \Im U$ as independent real-valued fields. Due to the linearity of the Fourier transformation, $\mathfrak{F}U = \mathfrak{F}p + \mathrm{i}\mathfrak{F}q$ holds. The free energy (12) is split into reciprocal-space and direct-space contributions:

$$\mathcal{F}[\psi, U] = \mathcal{F}_{\mathrm{rec}}[\mathfrak{F}\psi, \mathfrak{F}p, \mathfrak{F}q] + \mathcal{F}_{\mathrm{dir}}[\psi, p, q]. \tag{A.1}$$

The single contributions are

$$\begin{aligned}\mathcal{F}_{\mathrm{rec}}[\mathfrak{F}\psi, \mathfrak{F}p, \mathfrak{F}q] = \int \mathrm{d}^2k \,&\big(\big(B_{\mathrm{l}} + B_{\mathrm{x}}\big(-2k^2 + k^4\big)\big)\big)|\mathfrak{F}\psi|^2 \\ &+ \big(D + Ef\big(-k^2\big)\big)\big(|\mathfrak{F}p|^2 + |\mathfrak{F}q|^2\big) \\ &+ F\big(\mathfrak{F}p^* k_{\mathrm{R}} - \mathfrak{F}q^* k_{\mathrm{I}}\big)\mathfrak{F}\psi\big),\end{aligned} \tag{A.2}$$

$$\begin{aligned}\mathcal{F}_{\mathrm{dir}}[\psi, p, q] = \int \mathrm{d}^2x \,&\bigg(-\frac{1}{3}\psi^3 + \frac{1}{6}\psi^4 + \frac{1}{256}\big(p^2 + q^2\big)^2 \\ &+ \frac{1}{8}(\psi - 1)\psi\big(p^2 + q^2\big)\bigg),\end{aligned} \tag{A.3}$$

where $k_\mathrm{R} = \mathrm{i}^n \Re\big((k_x - \mathrm{i}k_y)^n\big)$ and $k_\mathrm{I} = \mathrm{i}^n \Im\big((k_x - \mathrm{i}k_y)^n\big)$. The functional derivatives of $\mathcal{F}_\mathrm{rec}$ are

$$\frac{\delta \mathcal{F}_\mathrm{rec}}{\delta \mathfrak{F}\psi^*} = 2\big(B_\mathrm{l} + B_\mathrm{x}\big(-2k^2 + k^4\big)\big)\mathfrak{F}\psi + Fk_\mathrm{R}{}^*\mathfrak{F}p - Fk_\mathrm{I}{}^*\mathfrak{F}q, \tag{A.4}$$

$$\frac{\delta \mathcal{F}_\mathrm{rec}}{\delta \mathfrak{F}p^*} = 2\big(D + Ef\big(-k^2\big)\big)\mathfrak{F}p + Fk_\mathrm{R}\mathfrak{F}\psi, \tag{A.5}$$

$$\frac{\delta \mathcal{F}_\mathrm{rec}}{\delta \mathfrak{F}q^*} = 2\big(D + Ef\big(-k^2\big)\big)\mathfrak{F}q - Fk_\mathrm{I}\mathfrak{F}\psi. \tag{A.6}$$

These are linear in $\mathfrak{F}\psi$, $\mathfrak{F}p$, and $\mathfrak{F}q$. In explicit Euler integration, the coefficients in these functional derivatives would be the elements of a matrix L. As in previous works [15], we deploy implicit Euler integration where possible, namely in (16). The integration step requires the inverse of the matrix

$$1 - \Delta t L = \begin{pmatrix} a & c_\mathrm{R}{}^* & -c_\mathrm{I}{}^* \\ c_\mathrm{R} & d & 0 \\ -c_\mathrm{I} & 0 & d \end{pmatrix} \tag{A.7}$$

with the elements as stated in (19) through (23). The functional derivatives of $\mathcal{F}_\mathrm{dir}$ are

$$\frac{\delta \mathcal{F}_\mathrm{dir}}{\delta \psi} = -\psi^2 + \frac{2}{3}\psi^3 + \frac{1}{8}(2\psi - 1)\big(p^2 + q^2\big), \tag{A.8}$$

$$\frac{\delta \mathcal{F}_\mathrm{dir}}{\delta p} = \frac{1}{64}\big(p^2 + q^2\big)p + \frac{1}{4}(\psi - 1)\psi p, \tag{A.9}$$

$$\frac{\delta \mathcal{F}_\mathrm{dir}}{\delta q} = \frac{1}{64}\big(p^2 + q^2\big)q + \frac{1}{4}(\psi - 1)\psi q. \tag{A.10}$$

ORCID iDs

Robert F B Weigel https://orcid.org/0000-0002-2919-9522
Michael Schmiedeberg https://orcid.org/0000-0001-7833-4906

References

[1] Cross M C and Hohenberg P C 1993 *Rev. Mod. Phys.* **65** 851
[2] Elder K R, Katakowski M, Haataja M and Grant M 2002 *Phys. Rev. Lett.* **88** 245701
[3] Elder K R and Grant M 2004 *Phys. Rev.* E **70** 051605
[4] Swift J and Hohenberg P C 1977 *Phys. Rev.* A **15** 319
[5] Alexander S and McTague J 1978 *Phys. Rev. Lett.* **41** 702
[6] Lifshitz R and Petrich D M 1997 *Phys. Rev. Lett.* **79** 1261
[7] Achim C V, Schmiedeberg M and Löwen H 2014 *Phys. Rev. Lett.* **112** 255501
[8] Ratliff D J, Archer A J, Subramanian P and Rucklidge A M 2019 *Phys. Rev. Lett.* **123** 148004
[9] Barkan K, Diamant H and Lifshitz R 2011 *Phys. Rev.* B **83** 172201
[10] Barkan K, Engel M and Lifshitz R 2014 *Phys. Rev. Lett.* **113** 098304
[11] Schmiedeberg M, Roth J and Stark H 2006 *Phys. Rev. Lett.* **97** 158304
[12] Rottler J, Greenwood M and Ziebarth B 2012 *J. Phys.: Condens. Matter* **24** 135002
[13] Wittkowski R, Löwen H and Brand H R 2011 *Phys. Rev.* E **83** 061706
[14] Löwen H 2010 *J. Phys.: Condens. Matter* **22** 364105

[15] Achim C V, Wittkowski R and Löwen H 2011 *Phys. Rev.* E **83** 061712
[16] Cremer P, Marechal M and Löwen H 2012 *Europhys. Lett.* **99** 38005
[17] Wang Z-L, Liu Z and Huang Z-F 2018 *Phys. Rev.* B **97** 180102
[18] Mkhonta S K, Vernon D, Elder K R and Grant M 2013 *Europhys. Lett.* **101** 56004
[19] Doye J P K, Louis A A, Lin I-C, Allen L R, Noya E G, Wilber A W, Kok H C and Lyus R 2007 *Phys. Chem. Chem. Phys.* **9** 2197
[20] Glotzer S C and Solomon M J 2007 *Nat. Mater.* **6** 557
[21] Pawar A B and Kretzschmar I 2010 *Macromol. Rapid Commun.* **31** 150
[22] Doppelbauer G, Bianchi E and Kahl G 2010 *J. Phys.: Condens. Matter* **22** 104105
[23] Bianchi E, Blaak R and Likos C N 2011 *Phys. Chem. Chem. Phys.* **13** 6397
[24] Doppelbauer G, Noya E G, Bianchi E and Kahl G 2012 *J. Phys.: Condens. Matter* **24** 284124
[25] van der Linden M N, Doye J P K and Louis A A 2012 *J. Chem. Phys.* **136** 054904
[26] Reinhardt A, Romano F and Doye J P K 2013 *Phys. Rev. Lett.* **110** 255503
[27] Gemeinhardt A, Martinsons M and Schmiedeberg M 2018 *Eur. Phys. J.* E **41** 126
[28] Gemeinhardt A, Martinsons M and Schmiedeberg M 2019 *Europhys. Lett.* **126** 38001
[29] Tracey D F, Noya E G and Doye J P K 2019 *J. Chem. Phys.* **151** 224506
[30] Romano F, Russo J, Kroc L and Šulc P 2020 *Phys. Rev. Lett.* **125** 118003
[31] Tracey D F, Noya E G and Doye J P K 2021 *J. Chem. Phys.* **154** 194505
[32] Noya E G, Wong C K, Llombart P and Doye J P K 2021 *Nature* **596** 367
[33] Sciortino F, Mossa S, Zaccarelli E and Tartaglia P 2004 *Phys. Rev. Lett.* **93** 055701
[34] Mladek B M, Gottwald D, Kahl G, Neumann M and Likos C N 2006 *Phys. Rev. Lett.* **96** 045701
[35] Lenz D A, Blaak R, Likos C N and Mladek B M 2012 *Phys. Rev. Lett.* **109** 228301
[36] Sciortino F and Zaccarelli E 2013 *Nature* **493** 30–1
[37] Thiele U, Frohoff-Hülsmann T, Engelnkemper S, Knobloch E and Archer A J 2019 *New J. Phys.* **21** 123021
[38] Subramanian P, Archer A J, Knobloch E and Rucklidge A M 2021 *IMA J. Appl. Math.* **86** 1164–80
[39] Stiakakis E *et al* 2021 *Nat. Commun.* **12** 7167
[40] Dotera T, Oshiro T and Ziherl P 2014 *Nature* **506** 208
[41] Fayen E, Jagannathan A, Foffi G and Smallenburg F 2020 *J. Chem. Phys.* **152** 204901
[42] Fayen E, Impéror-Clerc M, Filion L, Foffi G and Smallenburg F 2022 Self-assembly of dodecagonal and octagonal quasicrystals in hard spheres on a plane (arXiv:2202.12726)
[43] Rosenfeld Y 1989 *Phys. Rev. Lett.* **63** 980
[44] Hansen-Goos H and Roth R 2006 *J. Phys.: Condens. Matter* **18** 8413
[45] Roth R 2010 *J. Phys.: Condens. Matter* **22** 063102
[46] Roth R, Mecke K and Oettel M 2012 *J. Chem. Phys.* **136** 081101
[47] Neuhaus T, Schmiedeberg M and Löwen H 2013 *New J. Phys.* **15** 073013
[48] Neuhaus T, Marechal M, Schmiedeberg M and Löwen H 2013 *Phys. Rev. Lett.* **110** 118301
[49] Neuhaus T, Härtel A, Marechal M, Schmiedeberg M and Löwen H 2014 *Eur. Phys. J. Spec. Top.* **223** 373